

Synopsis: Closed-Loop Active Compensation for Needle Deflection and Target Shift During Cooperatively Controlled Robotic Needle Insertion

Patrick Donelan, Debbie Guenthner, Arjan Gupta, and Will Yingling

Abstract—Needle biopsies using intra-operative imaging assistance do not currently account for unmodeled needle deflection or target shift. Positional accuracy can be improved by rotating a bevel-tipped needle via a closed-loop image compensation controller. A physician-cooperative approach was used to increase patient-physician interaction while providing the physician with robot-assisted accuracy. Needle insertion tests were performed using this and a fully autonomous system to verify improvements in accuracy. The cooperative system showed no statistically significant difference in accuracy from the autonomous system, with an average accuracy of $3.56\text{mm}_{\text{rms}}$. The closed-loop control system was able to compensate for target shift up to the point where the error approached the maximum curvature possible for the needle. This shows that a cooperative, closed-loop control system during a needle biopsy can improve positional accuracy.

Index Terms—IEEE, IEEEtran, journal, L^AT_EX, paper, template.

I. INTRODUCTION

Accurate needle placement in deep percutaneous procedures such as targeted biopsy is critical to reducing procedure time, cost, and to increase patient comfort by reducing the need for multiple attempts. Intra-operative imaging can assist with this, but it does not account for unmodeled needle deflection or target shift. This can be compensated for by rotating a bevel-tipped needle according to a closed-loop image-guided control system. A fully autonomous needle insertion system is not desirable as it typically removes the physician entirely from patient contact, so a cooperative control system is presented. The physician applies an input force directly while the active compensation through needle rotation is performed autonomously.

This work was motivated by the robotics system described in Eslami *et al* [1]. While this system aligned the needle correctly, it still suffered from positional inaccuracy introduced by unmodeled needle deflection and target shift. The goal of this research is to implement a cooperative controlled needle correction system with closed-loop active compensation. This system must be compatible with an MR environment and have needle localization in real-time MR images as shown in Patel *et al* [2].

The error in needle accuracy due to deflection, and the amount of active compensation possible, is limited by the mechanical properties of the needle. Prior work to model this has been widely implemented using the kinematic bicycle

model [3] as well as a joint kinematic and dynamic system. [4] Other approaches ([5], [6]) use a duty-cycled approach for needle steering. This approach requires insertion and rotation to be tightly coupled, prohibiting cooperative control. Rossa *et al*, [7] presented a similar system with manual insertion and autonomous rotation, however it did not have a cooperative insertion approach, which increases the accuracy of the insertion axis as well.

A cooperative approach was chosen in this system to maintain physician interaction with the patient. Fully autonomous, isolated solutions are more likely to face increased regulatory scrutiny. [8] Teleoperated systems have been developed to address this issue ([9], [10], [11]). These systems often employ haptic or vibrational feedback to assist the physician in positioning the needle, however they still isolate the physician physically from the patient. A cooperative control scheme has the benefits of teleoperation while keeping the physician in the same room as the patient. There are many successful cooperative devices in use today ([12], [13], [14], [15]).

Prior work in steering needles via needle deflection has focused on thin, flexible needles which are not suitable for a clinical biopsy scenario. The approach presented here is focused on a clinical translation. *The primary contributions of this work are development of a method of closed-loop active compensation for unmodeled needle deflection and target shift under cooperatively controlled needle insertion, and experimental validation of this on an existing robotic needle placement system with results showing the accuracy improvements of autonomous needle placement can be maintained in user directed cooperative insertion.* [16]

II. METHODS AND MATERIALS

A. Workflow

The first step for image-guided feedback in cooperative needle insertion is to image a marker so a mapping from the image to the robot frame can be created. This mapping is then used to transform the insertion target into the robot frame so the robot can configure itself for a straight line insertion into the target. Once configured, the physician can initiate cooperative insertion. During insertion, the controller receives measurements of the needle tip location and target location, which are created from mapping positions in the image into the robot frame. The controller fuses these position measurements with measurements of the physician's input force along with a kinematic state transition model in order to determine the

velocity at which the needle should be inserted as well as how the tip should be oriented in order to closely adhere to the desired path. Control is terminated once the needle has been inserted to the desired depth or the needle has strayed too far from the desired path.

B. Needle Placement Manipulator

The robot used in this study included a 4-dof alignment base and a 2-dof cooperative control needle driver, resulting in a 6-dof system similar to that of [17] seen in Figure 1. The forces applied by the physician as well as the axial needle forces were measured using aluminum load cell sensors. Optical encoders were used to measure robot positions. The motors used for the base, needle insertion, and needle rotation were non-magnetic piezoelectric motors. The biopsy system that was used was the 18G175.

The sbRIO-9651 was the hardware used for the embedded control of the robot. The onboard FPGA was leveraged to handle low-level communication and the provided linux operating system was used for C/C++ development of the cooperative control algorithms. The controller was previously shown to work in MR environments by [18].

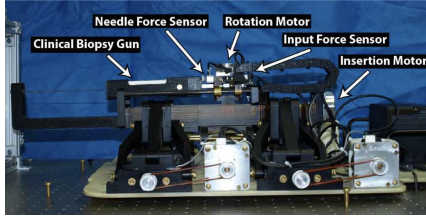


Fig. 1. Annotation of robot components

C. Cooperative Needle Insertion

The velocity of the needle insertion is calculated using the input force from the physician as well as the forces experienced by the needle, namely cutting force, tip stiffness, and friction [19] using Eq. (1). Thus, it is evident that the physician can control the insertion velocity through the force they apply. Insertion velocity profiles are illustrated for varying values of the decay constant λ in Figure 2. In the control system, if the desired insertion depth is reached, δF is set to 0. Once the desired velocity is calculated using Equation 1 a PID controller is used to maintain it.

$$v_{\text{insertion}} = \begin{cases} v_{\max} (1 - 0.9e^{-\lambda\delta F}) & \delta F > 0 \\ 0.1v_{\max} & \delta F < 0, F_{\text{input}} > 0 \\ 0 & \text{Otherwise} \end{cases} \quad (1)$$

where

$$\delta F = F_{\text{input}} - \sum F_{\text{needle}}$$

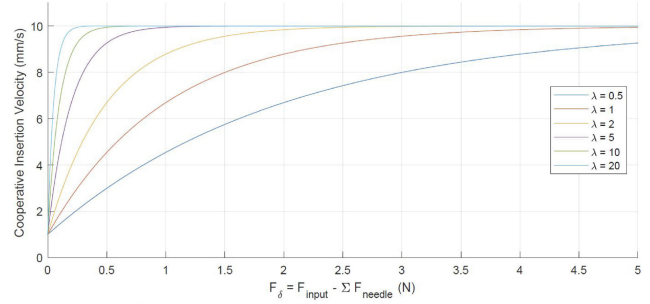


Fig. 2. Insertion velocity for varying λ

D. Feature Localization

We used two cameras to capture real-time images of the needle tip and target within the robot workspace. This is a suitable substitute for medical imaging, in fact the compensation technique is not dependent on the modality of the medical image. The two cameras are placed orthogonal to each other, and are run by a standalone software application.

In the software application, we employed Farnebäck's algorithm [20] to execute on captured video frames to localize the moving needle tip and obtain homogeneous transformations of the tip and the target. We used a color segmentation technique to demonstrate the active compensation.

E. Active Compensation

Before targeting, registration is performed by rigidly attaching a marker to the robot. For example, we would attach the marker with an MR visible object when moving through an MRI machine. This is visually supported by Figure 3.

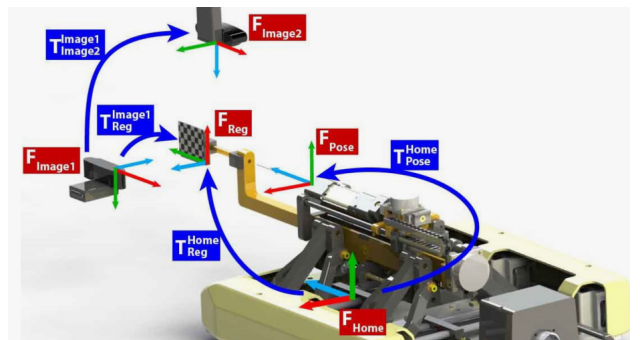


Fig. 3. Frames and transformations for image guidance registration

After the registration is complete, the marker is removed. The OpenIGTLINK [21] communication protocol is used to pass down the frame and transformations from image-guidance software to the robot controller. As seen by Figure 3, the transformation sequence $T_{\text{Pose}}^{H_{\text{Home}}} T_{\text{Reg}}^{H_{\text{Home}}} T_{\text{Reg}}^{I_{\text{Image}}}$ is used to express the registration with respect to the robot pose.

Throughout the insertion, the robot continuously receives the tip and target locations with respect to the image. Using the known transformation matrices, it determines the tip and target with respect to the robot pose. Naturally it can then compute the target location with respect to the tip, or $T_{\text{Target}}^{\text{Tip}}$. This tells us our desired compensatory effort.

To achieve this compensatory effort in all the insertion trials of our work, we chose to use Gang Li's novel CURV model [22], where both magnitude and direction of the desired effort can be implemented. Assume that θ is the current rotational angle of the bevel, and θ_d is the desired angle of the bevel for compensation. At any angular position, we can use the following equation.

$$\hat{\omega}(\theta, \theta_d) = 1 - \alpha e^{-\frac{(\theta-\theta_d)^2}{2c^2}} \quad (2)$$

Equation 2 gives the angular velocity as a function of θ and θ_d . Here, widening the Gaussian width c gives a bigger range of angles where rotation occurs below the nominal velocity. Also, increasing the Gaussian magnitude α leads to more deflection in θ_d . Gang Li's dissertation [22] can be consulted for the angular velocity profile graph of CURV. Also, while CURV was used in this work, it is possible to use other bevel tip based curvature models.

To calculate the θ_d in our case, we used the *atan2* function on the x and y positions obtained from T_{Target}^{Tip} . We set c is Equation 2 to 10° for all insertions. The α was chosen as an intermediate curvature value by projecting the needle tip orientation onto the target plane. For projecting the orientation, we first found the Euler angle rotation about the x and y axes, and then used the following equations,

$$X_{projected} = D_i \times \arctan(Rot(y)) \quad (3)$$

$$Y_{projected} = D_i \times \arctan(Rot(x)) \quad (4)$$

Where D_i is the remaining insertion depth. The x and y values of the current projection were also used to calculate the X_{error} and Y_{error} , which is the difference between the projection and target location. The overall error was given as,

$$Error_{projection} = \sqrt{(X_e + X_p)^2 + (Y_e + Y_p)^2} \quad (5)$$

where the subscript e signifies error, and subscript p signifies projection. Iterative values of α were calculated using the following,

$$\alpha = \frac{Error_{projected}}{Error_{max}} \quad (6)$$

III. RESULTS

A. Tissue Phantoms

Sampling tissue phantoms was developed and described in Hungr et al [23], Ahn et al [24] and Elayaperumal et al [25]. The same tissue phantoms were used in the following experiments to mimic needle forces in human-like tissue. Sampling tissue phantoms were made up of 70% Plastisol liquid PVC and PVC softener and 30% Regular Liquid Plastic and Plastic softener from M-F manufacturing (Fort Worth, TX, USA).

B. Accuracy for Stationary Targets

The first targeting experiment with static targets had to follow additional criteria to mimic needle forces to produce valid targeting accuracy results. Such as, the robot was positioned to place the needle tip at an entry point that will give a straight-line trajectory toward the target location and insertions were performed based on three conditions: (1) autonomous insertion with no rotation to characterize $Error_{max}$, which is the needle deflection without active compensation, (2) autonomous insertion with image-guided active compensation, and (3) hands-on user directed cooperative insertion with image-guided active compensation.

A ten-targeted insertion was used to test the hypothesis that targeting accuracy would improve with active compensation and the targeting accuracy would not be negatively affected when moving from an autonomous to cooperative insertion. All insertions were inserted until it reached the target depth and confirmed by visual confirmation of tip location using the needle tracking software. The results of experiment show the $Error_{max}$ was found to be 9.30 mm_{rms} for no compensation and 3.79 mm_{rms} for active compensation insertions. Testing on stationary target was determined that accuracy showed no statistically significant difference between autonomous insertions with active compensation and user directed cooperative insertions. The comparison of targeting accuracy of experiment is shown in Fig. 4. Across all insertions the average target depth was 125.23 mm_{rms} and the average targeting accuracy with active compensation was found to be 3.56 mm_{rms} .

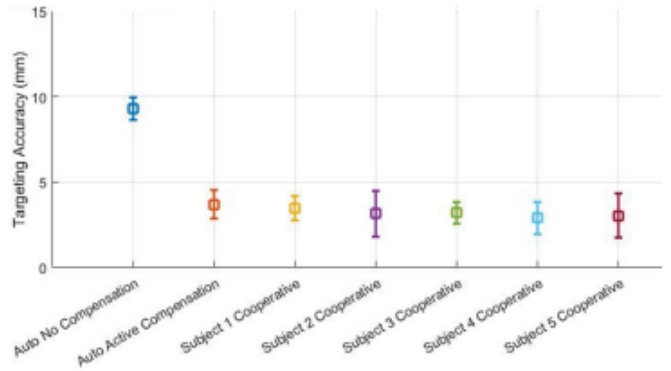


Fig. 4. Stationary Targeting Accuracy Insertions

C. Accuracy for Shifted Targets

The second targeting experiment with shifted target during cooperative insertions. The hypothesis was projected that $Error_{max}$ would be less than 9.30 mm_{rms} for no compensation since this was achieved with a static target. A twenty-targeted insertion was used to test this hypothesis in the same setup and tissue as the static experiment. The difference was once the needle contacted the phantom there was a target shift. The shift was virtually in the target plane perpendicular to the insertion axis, with both direction and magnitude assigned randomly. The range of direction was within 360° and magnitude between 1 and 10mm. The results of experiment show the $Error_{max}$ was found to be between 2.00 and 6.00 mm_{rms} .

D. Accuracy of Feature Localization

Validating the accuracy of feature localization to ensure the use of needle tracking outputs for robot control. A five-sample insertion was performed in the tissue as the two other experiments. The camera resolution was 640 x 480 pixels. The results of experiment showed that the error over the length of all insertions was 10.78 pixels_{rms} along the needle insertion path and 1.05 pixels_{rms} perpendicular to the insertion path. The phantom boundary was 2.65 and 0.12 mm_{rms}.

IV. DISCUSSION

For the feature localization and active compensation portions of the Materials and Methods, the synopsis authors hold high opinions about the procedure used by the original authors. Upon researching Farnebäck's algorithm [20], we concluded that it was indeed the best and perhaps most innovative way to localize the needle tip. The use of two cameras is also a clever approach. Furthermore, we were enamored by Gang Li's ingenious CURV technique [22] used to dynamically calculate the magnitude and direction of the error for closed-loop compensation. It was not necessary for the authors of the original paper to choose this bevel tip based curvature method, but the fact that it was shows the height of the innovation of this study.

REFERENCES

- [1] S. Eslami, W. Shang, G. Li, N. Patel, G. S. Fischer, J. Tokuda, N. Hata, C. M. Tempany, and I. Iordachita, "In-bore prostate transperineal interventions with an mri-guided parallel manipulator: system development and preliminary evaluation," *International Journal of Medical Robotics and Computer Assisted Surgery*, vol. 12, 2016.
- [2] N. A. Patel, T. V. Katwijk, G. Li, P. Moreira, W. Shang, S. Misra, and G. S. Fischer, "Closed-loop asymmetric-tip needle steering under continuous intraoperative mri guidance," vol. 2015–November, 2015.
- [3] R. J. Webster, N. J. Cowan, G. Chirikjian, and A. M. Okamura, "Non-holonomic modeling of needle steering," *Springer Tracts in Advanced Robotics*, vol. 21, 2006.
- [4] J. P. Swensen and N. J. Cowan, "Torsional dynamics compensation enhances robotic control of tip-steerable needles," 2012.
- [5] J. A. Engh, D. S. Minhas, D. Kondziolka, and C. N. Riviere, "Percutaneous intracerebral navigation by duty-cycled spinning of flexible bevel-tipped needles," *Neurosurgery*, vol. 67, 2010.
- [6] D. S. Minhas, J. A. Engh, M. M. Fenske, and C. N. Riviere, "Modeling of needle steering via duty-cycled spinning," 2007.
- [7] C. Rossa, N. Usmani, R. Slobooda, and M. Tavakoli, "A hand-held assistant for semiautomated percutaneous needle steering," *IEEE Transactions on Biomedical Engineering*, vol. 64, 2017.
- [8] S. K. Prasad, M. Kitagawa, G. S. Fischer, J. Zand, M. A. Talamini, R. H. Taylor, and A. M. Okamura, "A modular 2-dof force-sensing instrument for laparoscopic surgery," *Lecture Notes in Computer Science (including subseries Lecture Notes in Artificial Intelligence and Lecture Notes in Bioinformatics)*, vol. 2878, 2003.
- [9] Z. T. H. Tse, H. Elhawary, M. Rea, B. Davies, I. Young, and M. Lampert, "Haptic needle unit for mr-guided biopsy and its control," *IEEE/ASME Transactions on Mechatronics*, vol. 17, 2012.
- [10] D. Stoianovici, C. Kim, G. Srinathveeravalli, P. Sebrecht, D. Petrisor, J. Coleman, S. B. Solomon, and H. Hricak, "Mri-safe robot for endorectal prostate biopsy," *IEEE/ASME Transactions on Mechatronics*, vol. 19, 2014.
- [11] C. Pacchierotti, M. Abayazid, S. Misra, and D. Prattichizzo, "Teleoperation of steerable flexible needles by combining kinesthetic and vibratory feedback," *IEEE Transactions on Haptics*, vol. 7, 2014.
- [12] O. Schneider, J. Troccaz, O. Chavanon, and D. Blin, "Padyc: A synergistic robot for cardiac puncturing," *Proceedings-IEEE International Conference on Robotics and Automation*, vol. 3, 2000.
- [13] M. Jakopec, S. J. Harris, F. R. y Baena, P. Gomes, J. Cobb, and B. L. Davies, "The first clinical application of a "hands-on" robotic knee surgery system," *Computer Aided Surgery*, vol. 6, 2001.
- [14] A. Bettini, P. Marayong, S. Lang, A. M. Okamura, and G. D. Hager, "Vision-assisted control for manipulation using virtual fixtures," *IEEE Transactions on Robotics*, vol. 20, 2004.
- [15] G. Megali, O. Tonet, C. Stefanini, M. Boccadoro, V. Papaspypopoulos, L. Angelini, and P. Dario, "A computer-assisted robotic ultrasound-guided biopsy system for video-assisted surgery," vol. 2208, 2001.
- [16] M. Wartenberg, J. Schornak, K. Gandomi, P. Carvalho, C. Nycz, N. Patel, I. Iordachita, C. Tempany, N. Hata, J. Tokuda, and G. S. Fischer, "Closed-loop active compensation for needle deflection and target shift during cooperatively controlled robotic needle insertion," *Annals of Biomedical Engineering*, vol. 46, 2018.
- [17] M. Wartenberg, J. Schornak, P. Carvalho, N. A. Patel, I. I. Iordachita, C. M. Tempany, N. Hata, J. Tokuda, G. S. Fischer, J. B. M. U. Robotics, and S. Navigation, "Closed-loop autonomous needle steering during cooperatively controlled needle insertions for mri-guided pelvic interventions," 2017.
- [18] C. J. Nycz, R. Gondokaryono, P. Carvalho, N. Patel, M. Wartenberg, J. G. Pilitsis, and G. S. Fischer, "Mechanical validation of an mri compatible stereotactic neurosurgery robot in preparation for pre-clinical trials," in *2017 IEEE/RSJ International Conference on Intelligent Robots and Systems (IROS)*, 2017.
- [19] A. Okamura, C. Simone, and M. O'Leary, "Force modeling for needle insertion into soft tissue," *IEEE Transactions on Biomedical Engineering*, vol. 51, no. 10, pp. 1707–1716, 2004.
- [20] G. Farnebäck, "Two-frame motion estimation based on polynomial expansion," in *Proceedings of the 13th Scandinavian Conference on Image Analysis*, ser. SCIA'03. Berlin, Heidelberg: Springer-Verlag, 2003, p. 363–370.
- [21] J. Tokuda, G. S. Fischer, X. Papademetris, Z. Yaniv, L. Ibanez, P. Cheng, H. Liu, J. Blevins, J. Arata, A. J. Golby, T. Kapur, S. Pieper, E. C. Burdette, G. Fichtinger, C. M. Tempany, and N. Hata, "Openiglink: an open network protocol for image-guided therapy environment," *Int J Med Robot*, vol. 5, no. 4, pp. 423–34, 2009 Dec 2009.
- [22] G. Li, "Robotic system development for precision mri-guided needle-based interventions," 2016.
- [23] N. Hungr, J. A. Long, V. Beix, and J. Troccaz, "A realistic deformable prostate phantom for multimodal imaging and needle-insertion procedures," *Medical Physics*, vol. 39, 2012.
- [24] B. M. Ahn, J. Kim, L. Ian, K. H. Rha, and H. J. Kim, "Mechanical property characterization of prostate cancer using a minimally motorized indenter in an ex vivo indentation experiment," *Urology*, vol. 76, 2010.
- [25] S. Elayaperumal, J. H. Bae, B. L. Daniel, and M. R. Cutkosky, "Detection of membrane puncture with haptic feedback using a tip-force sensing needle," 2014.



Patrick Donelan Patrick Donelan received a B.S. in electrical engineering from Rensselaer Polytechnic Institute (Troy, NY) in 2021 with a concentration in robotics and automation. He is currently pursuing a M.S. in robotics engineering from Worcester Polytechnic Institute (Worcester, MA) with an expected graduation date in spring of 2026. He works full-time as an engineer for STR (Woburn, MA). At STR, he writes software for signal processing algorithms and simulations. His career interests are multi-agent control and swarm robotics.



Debbie Guenthner Debbie is employed with Infor as a Software Engineer. She graduated from Wichita State University in 2019 with Bachelor of Science in Computer Science. She is pursuing an understanding of robotic dynamics from Worcester Polytechnic Institute.



Will Yingling Will Yingling is employed as a software engineer with Spectra Logic Inc. He graduated from Colorado State University in 2019 with Bachelor of Science in Computer Science and a minor in mathematics. He is currently pursuing his Masters of Science in Robotics Engineering at Worcester Polytechnic Institute.



Arjan Gupta Arjan Gupta is an embedded software engineer employed by Lindsay Corporation. He graduated from the University of Kansas in May 2017 with a Bachelor of Science in computer engineering and a minor in mathematics. He is currently pursuing his Master of Science in robotics engineering at Worcester Polytechnic Institute.